The mechanical behaviour of vibrated, aerated beds of glass and starch powder

Janssen, L.P.B.M.; Marring, E.; Hoogerbrugge, J.C.; Hoffmann, A.C

Published in:
Chemical Engineering Science

DOI:
10.1016/S0009-2509(97)00375-8

Publication date:
1998

Pergamon

Chemical Engineering Science, Vol. 53, No. 4, pp. 761–772, 1998

Printed in Great Britain
PII: S0009-2509(97)00375-8
0009-2509/98 $19.00 + 0.00

The mechanical behaviour of vibrated, aerated beds of glass and starch powder

L. P. B. M. Janssen, E. Marring, J. C. Hoogerbrugge and A. C. Hoffmann*

Department of Chemical Engineering, University of Groningen, Nijenborgh 4, 9747 AG Groningen, The Netherlands

(Received 22 May 1997; accepted 17 October 1997)

Abstract—A model which describes the movement of a powder bed subjected to vibration and aeration through a porous support plate is proposed and solved. The calculated bed movement is shown graphically both as a function of time and — taking discrete Fourier transforms — of frequency. To validate the model experimentally, a new experimental technique was developed. This involved measuring the movement of a porous disc inserted in the bed and following the bed movement. The methodology and the difficulties involved are discussed. The experimental results are presented as Fourier transforms of the bed movement. Both model and experiment show that at the higher vibration intensities, where the bed looses contact with the support plate, bed movement with a period of more than one vibration cycle causes the appearance of a peak in the Fourier spectrum at half the plate excitation frequency. The intensity at which this first occurs is acceptably well predicted by the model. On the whole, taking into account the assumptions made in the model and unavoidable experimental errors, predictions and experimental results show good agreement. © 1998 Elsevier Science Ltd. All rights reserved

Keywords: Vibration; aeration; fluidization; powder bed; model.

INTRODUCTION AND LITERATURE SURVEY

The application of vibration makes it possible to process cohesive powders, otherwise not amenable to fluidization, in the fluidized state (e.g. Marring *et al.*, 1994). Since one of the major advantages of fluidized beds above packed beds is the ability to process sticky or wet particulate materials, vibration as a means of extending the range of applicability of fluidization even further is very advantageous. Vibrated fluidized beds are used throughout the processing industry. Applications span physical operations such as (freeze) drying, heating, cooling, granulation and crystallization and a wide range of chemical operations.

In spite of this, most of the modelling efforts for vibrated powder beds in the research literature are concerned with non-aerated beds vibrated on an impermeable plate. The literature considering aeration is very limited.

When a bed of powder is subjected to vertical vibration, it will, at low vibration intensities, remain in contact with the distributor plate. At higher vibration intensities where the downwards acceleration of the vibrated support plate exceeds that of the bed at some point in the cycle, an air gap between bed and plate is formed (the bed is 'in flight'). Most of the research literature concentrates on this latter region, where the shocks from impacts between bed and support plate cause break-up of particle–particle bonds, beneficial for the fluidization and handling of the powder.

Modelling of non-aerated beds vibrated on an impermeable plate

The simplest model is that of the bed moving as a coherent piston taking into account only the influence of gravity when the bed is in flight [sometimes referred to as the 'one particle' model, Takahashi *et al.* (1968/69)]. In this model the effect of air drag on the moving bed is thus neglected.

However, the gas permeating the bed while it is in flight (due to the change in volume of the air gap between bed and support plate) adds a drag force to the gravitational force. This was accounted for in the models of Kroll (1954) and Yoshida and Kousaka (1967). They assumed the interstitial gas to be incompressible, and therefore that the axial pressure gradient in the bed is linear. Kroll also showed that the pressure gradient in many practically relevant cases may deviate significantly from the linear.

Gutman (1976a) and Akiyama and Naito (1987) allowed for the interstitial gas to be compressible. Both solved the model equations of Gutman analytically using different methods. In order to do this they

*Corresponding author.

made assumptions about the functional form of the bed and support plate movement and the axial pressure profile in the bed.

Modelling of aerated beds

Kavetskii *et al.* (1976) and Erdész and Halász (1984) modelled the movement of a vibrated, aerated bed. They made the assumption of incompressible interstitial gas.

Yamazaki *et al.* (1974) allowed for compressibility of the interstitial gas in their model for a vibrated, aerated bed. However, they assumed a sinusoidal bed movement.

Experimental methods for determining the movement of vibrated, non-aerated beds

Most experimental methods concentrate on the air gap developing at higher vibration intensities. Visual observation by means of a stroboscope was used by Kroll (1954), Gray and Rhodes (1972), Wes (1984) and Thomas *et al.* (1987). Some of these workers used high speed photography to record the observed data.

More detailed knowledge about the bed motion can be gained by photographing the air gap using a flash with an adjustable phase lag with the imposed vibration. This technique was used by Kroll (1954), Pakowski and Strumillo (1980) and Thomas *et al.* (1987).

Gutman (1976b) measured the capacitance between two plates placed on each side of the lower part of a two-dimensional fluidized bed. Gray and Rhodes (1972) used a bed of electrically conducting material and measured the conductivity between bed and support plate. In this way the presence of an air gap, but not its size, could be established.

Objectives of this work

The survey above shows that the models taking into account bed aeration are based on the assumptions either of incompressible interstitial gas or a sinusoidal bed movement. It will be clear from what follows that the first of these assumptions is not even approximately true for the case studied here, and that the second precludes a sufficient description of the bed movement precisely in the interesting range of vibration intensities, where the bed looses contact with the support plate. The objective of the work reported in this article is to formulate a model for the movement of a vibrated powder bed including the effect of aeration through a porous distributor plate, and to verify this model experimentally. Particular attention will be paid to the range of vibration intensities and aeration rates where the bed looses contact with the distributor plate and the periodic impact of bed and plate gives rise to shocks breaking up particle bonds and channels.

EFFECT OF THE DIFFERENT MODELLING ASSUMPTIONS ON THE PREDICTED BED MOVEMENT

In this section our own calculations will be used to illustrate the effect of some of the modelling assumptions mentioned in the previous section.

The movement of the vibrating support plate is assumed sinusoidal with amplitude x_o and angular frequency ω, so that its displacement, x_{pl}, is given by:

$$x_{pl} = x_o \sin(\omega t). \tag{1}$$

We define a parameter, the so-called vibration number, G, which compares the maximal acceleration of the plate with that due to gravity, g:

$$G = x_o \omega^2 / g. \tag{2}$$

In the 'one particle' model, the bed looses contact with the support plate for $G > 1$. During the subsequent flight, the bed movement is ballistic. The time of collision with the plate, t_o, can be calculated iteratively. After the (inelastic) collision, the bed follows the plate.

We define dimensionless plate and bed displacements, X_{pl} and X_b, in terms of x_o:

$$X_{pl} \equiv x_{pl}/x_o, \qquad X_b \equiv x_b/x_o \tag{3}$$

and a dimensionless time by dividing by the plate cycle period. The subscripts b and pl refer to the bed and plate, respectively.

Figures 1 and 2 show calculated dimensionless bed displacements in the dimensionless time and in the frequency domains, respectively, at a series of values of G using the 'single particle' model. In Fig. 1, the plate displacement is represented by the sinusoidal curve.

For $G \leqslant 1$ (this is not shown in the figure) the bed follows the plate, and the Fourier spectrum displays only a peak at the excitation frequency of 30 Hz. At $1 \leqslant G \leqslant 3.3$, a gap between plate and bed develops, and the bed falls back within one cycle. The peaks at the higher harmonics in the Fourier spectrum are due

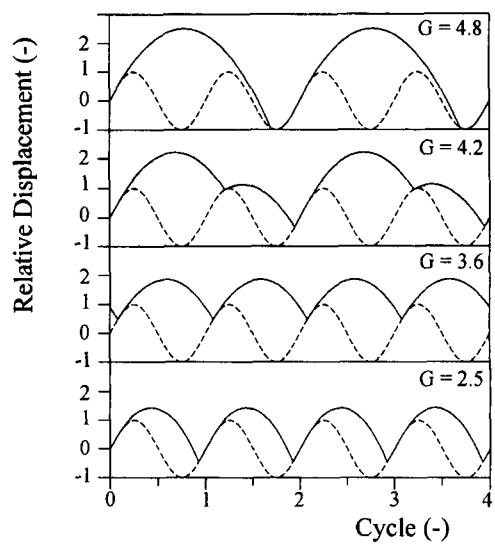

Fig. 1. Relative plate and bed displacement according to the one-particle model for different vibration numbers at $f = 30$ Hz.

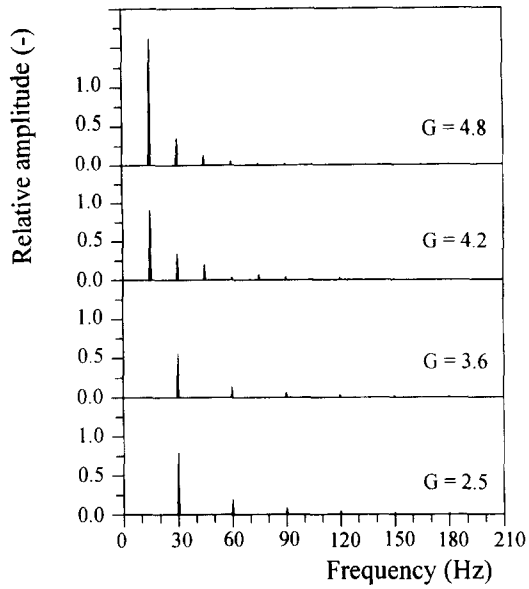

Fig. 2. Fourier analysis of the relative bed displacement according to the one-particle model for different vibration numbers at $f = 30$ Hz.

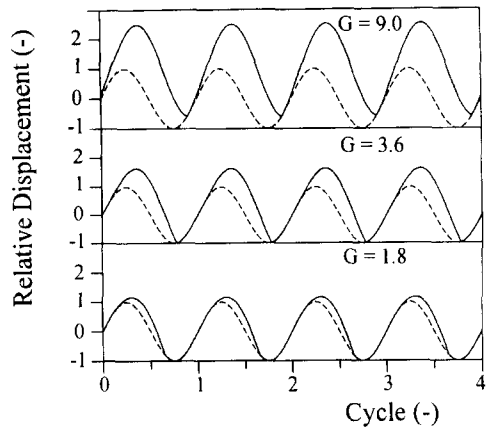

Fig. 3. Relative plate and bed displacement calculated from the model equations of Gutman for different vibration numbers; $f = 30$ Hz, $H_b = 0.25$ m, $d = 65.8$ μm.

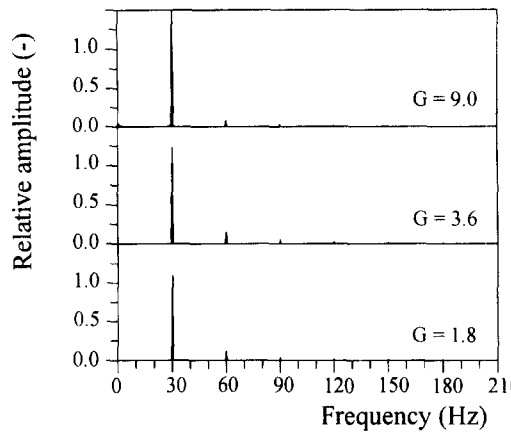

Fig. 4. Fourier analysis of the relative bed displacement calculated from the model equations of Gutman for different vibration numbers at $f = 30$ Hz, $H_b = 0.25$ m, $d = 65.8$ μm.

to the bed movement not being sinusoidal. For $3.3 \leqslant G \leqslant 3.9$, the bed movement shows irregularity on a long time scale (not clear from this figure). In the region $3.9 \leqslant G \leqslant 4.2$, the bed movement again appears roughly regular, but the periodicity of the bed movement is seen to span two cycles of the plate movement, resulting in the strong peak at half the plate excitation frequency in the Fourier spectrum. When G exceeds 4.6, the bed is thrown over the top of every other plate cycle, and only contacts the plate with half the frequency.

In order to demonstrate the effect of drag on a vibrated bed, calculations were performed using the model equations of Gutman (1976a). The model powder is one of the powders used experimentally (see later): glass ballotini with particle density, ρ_p, 2850 kg/m^3, surface/volume mean diameter, d, 65.8 μm and bed voidage, ε_b, 0.37. The results are shown in Figs 3 and 4. The plots corresponding to $G = 3.6$ can be compared with the corresponding ones in Figs 1 and 2, where drag is not included. It can be seen that drag has the effect of drawing the bed to the plate during flight, so that the bed follows the plate movement more closely. Even at $G = 9.0$, the bed is still attracted so strongly that the bed is not thrown over the following highest plate position.

In the course of these calculations of the bed movement, the pressure profile in the bed is also calculated at each time step (see below). Some profiles after the passage of 30 cycles are shown in Fig. 5. It is clear how the underpressure in the developing air gap is reversed into an overpressure as the gap closes again. It is also clear that the pressure variation is non-linear in this case and limited to the lower region of the bed.

This has demonstrated the effects of the parameters involved. The calculations have also made clear that the models for a bed vibrated on a non-porous support plate are not sufficient to describe a bed vibrated on a porous support plate, whether aerated or not, since air entering the developing air gap through the porous support plate in most practical cases will have a significant effect on the bed movement.

A MODEL FOR A RIGID, POROUS PISTON ON A VIBRATING POROUS PLATE WITH AERATION

The situation modelled is sketched in Fig. 6. Aeration is supplied to a wind-box of fixed volume and enters the bed though a porous support plate. Friction with the walls of the bed is neglected and the bed porosity is assumed constant.

The strategy is to solve the equation of motion of the bed while in flight, evaluating the drag on the bed from the instantaneous pressure in the air gap. As the

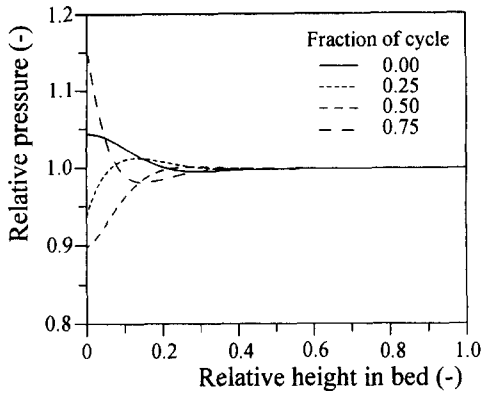

Fig. 5. Axial pressure distribution calculated from the model equations of Gutman, $f = 30$ Hz, $G = 3.6$, $H_b = 0.25$ m, $d = 65.8$ μm.

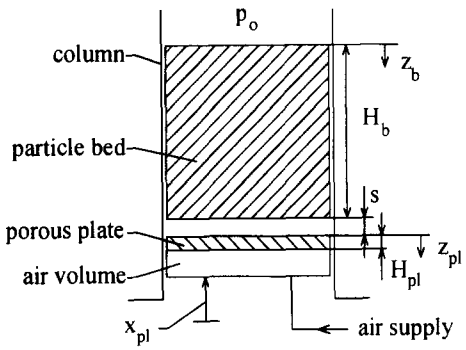

Fig. 6. The vibrated powder bed with aeration.

gap increases, the pressure in it is reduced and air is sucked in from (and, if the bed is permeable enough: through) the bed and through the distributor plate, and conversely when the gap reduces. The pressure in the air gap can therefore be found by a numerical calculation of the axial pressure profile in the bed and the porous support plate at each time step. Since the pressure profile is unsteady, it also has to be evaluated during the intervals where the bed is in contact with the support plate.

The equation of motion for the bed in flight is

$$\rho_b H_b A_b \frac{d^2 x_b}{dt^2} = -\rho_b H_b A_b g + (p_{z_b = H_b} - p_o) A_b \quad (4)$$

where ρ_b is the bulk density of the bed, A_b and H_b the bed cross-sectional area and height, p is the pressure, p_o atmospheric pressure and t time. z_b is an axial coordinate fixed to the bed. Equation (4) equates the mass times acceleration of the bed (on the RHS) to the forces acting on it arising from gravity (first term on the LHS) and the pressure drop (or drag, the second term on the LHS). In terms of the height of the air gap, $s = x_b - x_{pl}$:

$$\frac{d^2 s}{dt^2} = -g + \frac{(p_{z_b = H_b} - p_o)}{\rho_b H_b} + x_o \omega^2 \sin(\omega t) \quad (5)$$

If the bed is not in flight, eq. (5) reduces to $d^2 s/dt^2 = 0$. Equation (5) contains the pressure in the air gap which is evaluated as follows.

The percolation of gas through the bed is assumed to follow Darcy's law:

$$v = -\frac{k_b}{\mu} \frac{\partial p}{\partial z_b} \quad (6)$$

with v the superficial gas velocity, k_b the bed permeability and μ the dynamic viscosity of the gas. The applicability of Darcy's law for this application was validated by Gutman and Davidson (1975). The continuity equation for the interstitial gas in the bed is

$$\frac{\partial}{\partial t}(\varepsilon_b \rho) = \frac{\partial}{\partial z_b}(\rho v) \quad (7)$$

with ε_b the voidage of the bed and ρ the gas density. Inserting a constitutive equation (e.g. the ideal gas law) herein would result in an equation for the pressure, but it would be a non-linear one. This problem can be avoided by assuming that the relative variation in gas velocity greatly exceeds that of the gas density in the axial direction:

$$\left| v \frac{\partial \rho}{\partial z_b} \right| \ll \left| \rho \frac{\partial v}{\partial z_b} \right|. \quad (8)$$

An order of magnitude calculation indicates that the fluctuations in v are about 10 times the mean value, while those in ρ are only about 20% of the mean value (this can be inferred from the pressure fluctuations shown in Fig. 5); the fluctuations in both variables are over a similar length scale. We can then put the gas density outside the differential on the RHS of (7) using ρ_o, the gas density at atmospheric conditions, there. As constitutive equation we use the ideal gas law:

$$p = \rho RT/M. \quad (9)$$

Inserting Eqs (6) and (9) in eq. (7) under the assumption (8) gives an equation for the pressure distribution in the bed:

$$\frac{\partial p}{\partial t} = \frac{p_o k_b}{\varepsilon_b \mu} \frac{\partial^2 p}{\partial z_b^2} = \alpha \frac{\partial^2 p}{\partial z_b^2}. \quad (10)$$

This equation has the form of a diffusion equation, and defines a 'diffusivity', α. It is a second degree equation, so we need boundary condition at the top and bottom of the bed. At the top of the bed:

$$z_b = 0; \quad p = p_o \quad (11)$$

and at the bottom of the bed we use a continuity equation for the gas in the air gap (see Fig. 6):

$$\frac{d(\rho s)}{dt} = -\rho \frac{k_b}{\mu} \left(\frac{\partial p}{\partial z_b} \right)_{z_b = H_b} + \rho \frac{k_{pl} A_{pl}}{\mu A_b} \left(\frac{\partial p}{\partial z_{pl}} \right)_{z_{pl} = 0}. \quad (12)$$

The first term on the RHS of eq. (12) is the same as the term of Gutman (1976a), the second is our term accounting for the porosity of the support plate. The problem here again is that inserting for ρ from a

constitutive equation gives a non-linear boundary condition. We follow Gutman in assuming:

$$\left|s\frac{\partial\rho}{\partial t}\right| \ll \left|\rho\frac{\partial s}{\partial t}\right|. \tag{13}$$

An order of magnitude calculation shows that this assumption by no means is a triviality. In the present case the right-hand side exceeds the left-hand side by an order of magnitude. The assumption may be invalid in systems where the bed and plate are very dense, causing ρ to fluctuate violently. Using eq. (13) a linear boundary condition is obtained:

$$\frac{ds}{dt} = -\frac{k_b}{\mu}\left(\frac{\partial p}{\partial z_b}\right)_{z_b=H_b} + \frac{k_{pl}A_{pl}}{\mu A_b}\left(\frac{\partial p}{\partial z_{pl}}\right)_{z_{pl}=0}. \tag{14}$$

The pressure in the support plate is also described by eq. (10), only with the subscript b substituted with pl. The boundary condition at the top of the support plate is eq. (14), and the boundary condition at the bottom is the continuity of gas over the wind-box (see Fig. 6):

$$z_{pl} = H_{pl}: \frac{\partial p}{\partial t} = \frac{p_o\varphi_v}{V_{pl}} - \frac{p_o k_{pl}A_{pl}}{V_{pl}\mu}\frac{\partial p}{\partial z_{pl}} \tag{15}$$

where φ_v is the volumetric air supply rate, V_{pl} the volume of the wind-box and A_{pl} the area of the support plate.

The equations for the pressure profiles in the bed and support plate with their boundary conditions are valid whether the bed is in flight or not. If the bed is not in flight, $ds/dt = 0$ can be inserted in boundary condition (14).

PARAMETER ESTIMATION AND MODEL PREDICTIONS

The numerical method of solution of the model equations is described in Appendix A. The aeration rate has as upper limit the minimum fluidization velocity of the powder bed. For the fine powder considered here, the bed permeability can be calculated from:

$$k_b = \frac{d^2\varepsilon_b^3}{180(1-\varepsilon_b)^2} \tag{16}$$

where d is the surface/volume mean diameter of the bed particles. Putting the buoyant weight of the bed per unit area equal to the pressure drop over it gives an expression for v_{mf}, the superficial gas velocity at conditions of minimum fluidization:

$$v_{mf} = \frac{d^2\varepsilon_b^3\rho_p g}{180\mu(1-\varepsilon_b)}. \tag{17}$$

Most of the model calculations were performed using the physical characteristics of the bed and support plate used for experimental work described in the following section. The bed parameters are: $d = 65.8\ \mu m$, $\varepsilon_b = 0.37$, $\rho_p = 2850\ kg/m^3$, $H_b = 0.25\ m$ and $A_b = 0.0651\ m^2$. The support plate parameters are: $k_{pl} = 2.0\times10^{-13}\ m^2$, $\varepsilon_{pl} = 0.28$, $H_{pl} = 0.002\ m$, $A_{pl} = 0.0506\ m^2$ and $V_{pl} = 1.78\times10^{-3}\ m^3$.

We now use the model to give a short account of the predicted effect on the bed behaviour of aeration through a porous plate, and compare with the behaviour of a bed vibrated on an impermeable support plate.

The effect of varying the aeration rate is shown in Figs 7 and 8. The dimensionless aeration rate is defined as: $V \equiv (v/v_{mf})$. The air gap widens for higher aeration rates, while the frequency of the bed movement remains the same as for the plate, there are therefore no undertones visible in the Fourier spectrum. The deviation from the sinusoidal of the bed movement gives rise to peaks at higher harmonics in the spectrum.

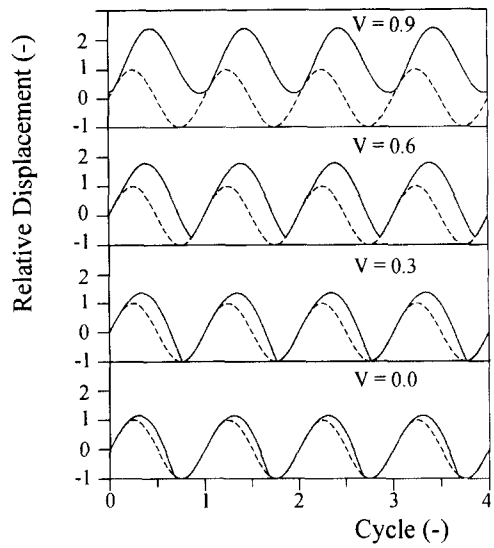

Fig. 7. Relative plate and bed displacement for different aeration rates, $f = 30$ Hz, $G = 1.8$, calculated by the model.

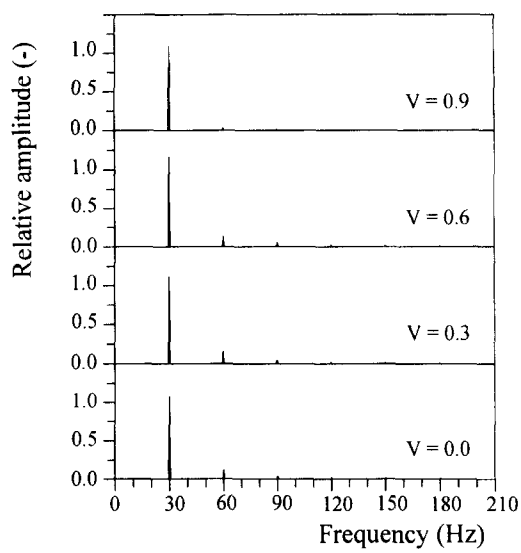

Fig. 8. Fourier analysis of the model predictions of the relative bed displacement for different aeration rates, $f = 30$ Hz, $G = 1.8$.

The bottom parts of Figs 3 and 7 can be compared since they are generated under the same vibration conditions. One would expect a longer bed flight due to the porosity of the support plate in Fig. 7. However, since the permeability of the support plate is one order of magnitude less than that of the bed in this case, the difference is only slight. In other cases the difference will be quite substantial.

In Figs 9 and 10, the vibration frequency is varied at a constant aeration rate of $V = 0.9$. The trends for the two lowest frequencies are the same as for no aeration. At 60 Hz, however, a cyclic pattern repeating every two plate periods is evident. A corresponding peak in the Fourier spectrum at half the excitation frequency of the support plate is visible.

In the subsequent sections we describe experimental work and compare the results of this with the predictions of the model.

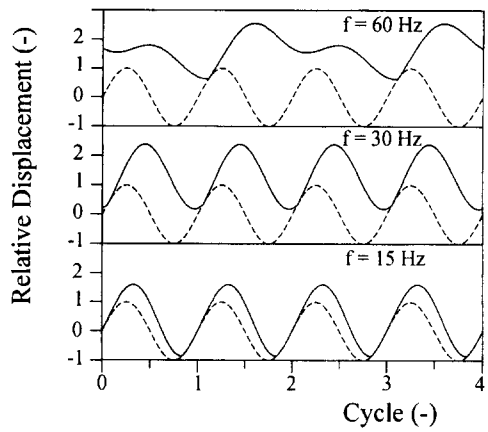

Fig. 9. Relative plate and bed displacement for different frequencies by a constant aeration rate according to the model, $G = 1.8$, $V = 0.9$.

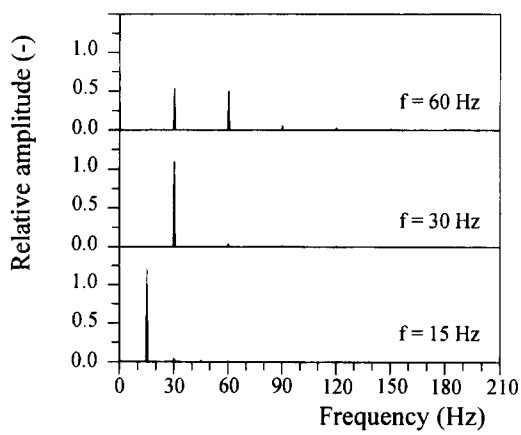

Fig. 10. Fourier analysis of the model predictions of the relative bed displacement for different frequencies by a constant aeration rate according to the present model, $G = 1.8$, $V = 0.9$.

EXPERIMENTAL

Photographic techniques do not allow easy data handling, and capacitance and conductivity methods only give indirect information about the bed movement. A new experimental method was therefore developed. The equipment is shown in Fig. 11.

The columns was made of perspex with a diameter of 0.288 m and a height of 0.414 m. The support plate was a porous metal plate with the following measured properties: permeability, k_{pl}: 2.0×10^{-13} m^2, voidage, ε_{pl}: 0.28, height (thickness), H_{pl}: 0.002 m, surface area, A_{pl}: 0.0506 m^2 (this is the free area). The volume of the gas box, V_{pl} is 1.78×10^{-3} m^3. A rubber seal between the movable support plate and the column prevented leakage of air and powder. The air flow rate was measured by critical flow nozzles.

The powders used were glass ballotini (diameter range: 35–80 μm, volume/surface mean diameter, d_{sv}: 65.5 μm, density, ρ_p: 2850 kg/m^3 and packed bed voidage, ε_b: 0.37) and native potato starch with a water content of 6% on dry solids basis (diameter range: 7–100 μm, volume/surface mean diameter, d_{sv}: 34.6 μm, density, ρ_p: 1513 kg/m^3 and packed bed voidage, ε_b: 0.40). The latter powder was cohesive.

The movement of the bed material was recorded by a porous disc moving with the bed. The pores in the disc were relatively large (200–500 μm) and penetrable for the bed material, in order to make it compatible in terms of permeability and bulk density with the surrounding bed. Experimentation proved a disc diameter of 90 mm to be optimal, while the thickness was 5.5 mm. The movement of the disc was passed to a 'linear variable differential transformer' (LVDT) by means of a connecting rod. It was then filtered (see Appendix B), sampled and digitized for processing in the data logging computer. The weight of the connecting rod and the plate were compensated by a counterweight. The frame holding the LVDT could be

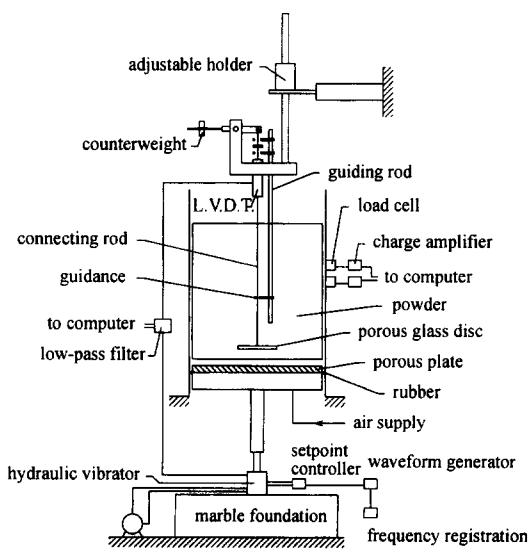

Fig. 11. Experimental set-up

adjusted in position and was loose from the frame holding the bed to eliminate disturbances.

One great advantage of this method is that the movement in the internal regions of the bed could be measured. The methods used by other researchers only allow observation of the movement at the wall.

The hydraulic vibrator was mounted on a heavy marble foundation. The column was attached to a frame clamped between the floor and the ceiling in order to eliminate vibration in the column itself. The amplitude and frequency of the vibration of the plate was controlled using a setpoint controller and a waveform generator, respectively. The large and varying forces exercised by the moving bed on the support plate disturbed the waveform of the hydraulic vibrator. It was, therefore, necessary to record the plate movement in a second LVDT and pass it continuously in a feedback loop to the setpoint controller, which performed corrective adjustments to maintain a sinusoidal plate motion.

Vibration frequencies up to 100 Hz were tested experimentally. In order to include any higher harmonics in the analyses, frequencies up to 500 Hz were measured. Any frequencies above this were filtered out by a low-pass filter as shown in the diagram. The sampling frequency was set to 1024.6 Hz (see also Appendix B).

The LVDT's were calibrated statically measuring the output voltage for different displacements. However, calibration under dynamic conditions was also necessary to determine a possible influence of other factors, such as give in the mechanical connections. In order to do this, the connecting rod was fastened to the support plate and the output from the two LVDT's compared both with the bed vessel empty and with a bed of glass ballotini in it. With the bed vessel empty, the two agreed to within 5% under all conditions, which proves the accuracy of both measuring systems. With bed material in the vessel the deviation between the two was somewhat larger. Figure 12 shows the ratio of the amplitude registered by the displacement measuring system to that of the support plate. With no aeration of the bed the difference becomes significant above frequencies of 60 Hz. With aeration at minimum fluidization conditions, the difference is within 13% at all conditions, and within 5% for vibration frequencies below 60 Hz.

The general conclusion is that the displacement measurements are reasonably good for low vibration frequencies, but that deviation from the static calibration should be taken into account when evaluating the results, particularly at vibration frequencies above 60 Hz.

The processing of the signals coming from the LVDT recording the bed movement will be described in Appendix B.

RESULTS AND COMPARISON WITH THEORY

In this section the Fourier transforms of $X_b(t)$, calculated as set out in Appendix B, will be shown. The peak at zero Hz, and the one at 50 Hz, representing the disturbance from the net supply, are not shown.

Experiments without aeration

Without aeration, measurements were limited to moderate vibration intensities, since the disc measuring the bed movement would move out of position at high intensities.

Figure 13 shows the ratio of bed to plate amplitude as a function of frequency for a bed of glass ballotini (height 0.248 m) and of native potato starch (height 0.261 m) at $G = 1$. In spite of the fact that the bed should remain in contact with the plate under these conditions, and the ratio should therefore be as close to unity as in Fig. 12, it differs significantly from this value. The pattern of the deviation is almost identical for the two beds in spite of their very different mechanical properties, eliminating elastic deformation of the beds as a cause of the deviation. Moreover, the deviation showed an almost identical pattern when similar measurement were performed at other axial positions in the beds. The exact cause of this phenomenon will have to be investigated further. On basis of the evidence, the discrepancy is most likely to be

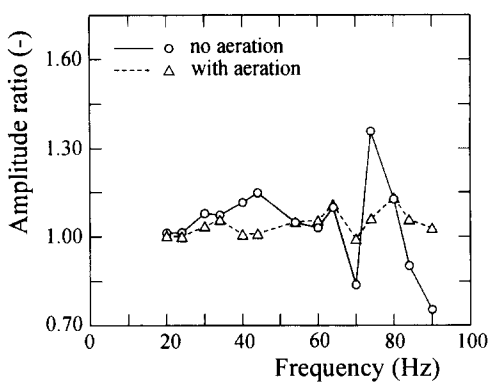

Fig. 12. Check on the calibration of the displacement measurement system under dynamic conditions without and with aeration for a bed of glass ballotini at $G = 1.0$.

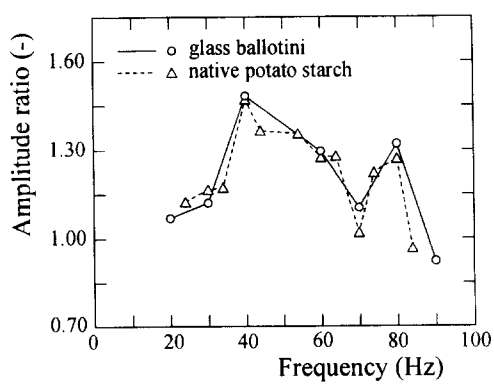

Fig. 13. Amplitude ratio without aeration for different frequencies at $G = 1.0$.

caused by friction between the bed material on the one hand and the guiding rod/guidance on the other (see Fig. 11), causing movement in the frame holding the LVDT. If this is so, the errors should be much reduced as soon as aeration is applied, since friction with solid objects is known rapidly to be reduced when a powder bed is aerated. One conclusion which can be drawn from these measurements is that the movement of the material at different heights in the bed is essentially the same under these conditions.

Without aeration, the bed of glass ballotini was subjected to vibration in the range 20–90 Hz, while G was varied by means of the vibration amplitude. Only at 90 Hz could G be raised to such a level that a peak at half the excitation frequency appeared. The corresponding Fourier spectra are shown in Fig. 14. The disc was located at 9 cm above the support plate in these experiments. The peaks at half the frequency of the support plate at the two highest values of G shows that the bed movement is repeating itself every two cycles. Notice the very strong non-frequency specific noise evidenced by the undulating sprectrum especially in the bottom part of this figure. Showing the results as Fourier spectra makes it possible to identify and emphasize only the relevant information about the bed movement.

Our calculations show that the model including air drag and, conspicuously, even the one-particle model predict no undertones at any of the conditions shown in Fig. 14. Perhaps the wall friction contributed to the early appearance of the undertones. Wall friction was, in fact, measured and will be discussed below. If wall friction is, indeed, the reason for the discrepancy between model and experiment, the agreement should be better when aeration is applied, since the wall friction is then reduced.

While undertones appeared in the bed of glass ballotini at $G = 2.0$, other experiments showed that they did not appear until $G = 2.5$ in a bed of potato starch of a similar height also vibrated at a frequency of 90 Hz. This difference is consistent with the air drag holding the latter bed in closer contact with the support plate, the bed being less permeable and also lighter than the bed of glass ballotini.

Experiments with aeration

For the bed of glass ballotini the vibration frequency was kept fixed at 30 Hz, while G was varied in the range 0.2–1.75, and various aeration rates were used for each value of G. The bed behaviour at $G = 1.25$ is representative, and is shown in Fig. 15. The bed behaviour predicted by our model is shown in Fig. 16.

Comparing the two figures, agreement between experiment and model predictions is seen. In both cases peaks at the higher harmonics arise due to deviation of the bed movement from the sinusoidal, and peaks at half the excitation frequency arise at the higher vibration intensities. Experiments using potato starch showed the same trends and the same agreement with the model predictions.

We may therefore conclude that the model describes the system with aeration well: qualitatively, the agreement is excellent, and quantitatively the discrepancy between model and experiment is only slight. In the following section we discuss some features of the system not accounted for in the model, but which may be of significant influence and, if included, may improve the predictive power of the model.

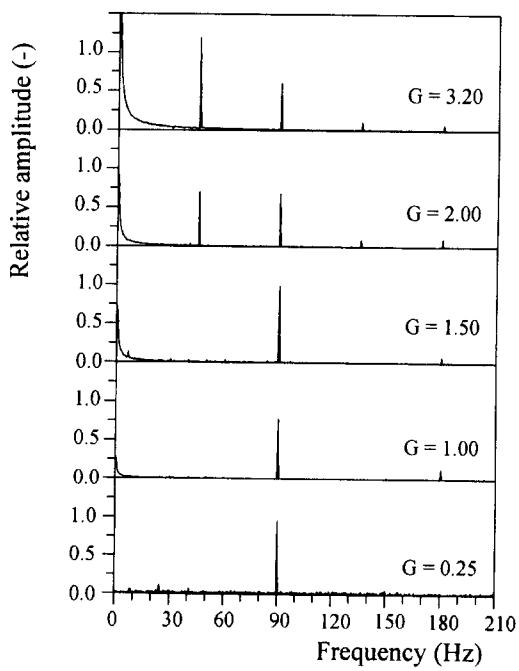

Fig. 14. Fourier analysis of the measured relative bed displacement for different vibration numbers: glass ballotini, $f = 90$ Hz.

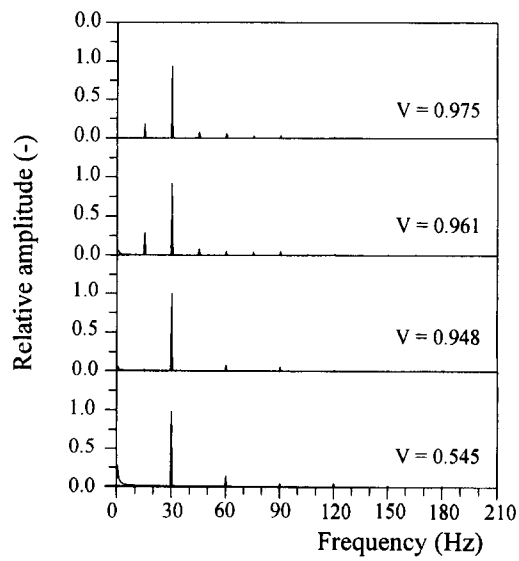

Fig. 15. Fourier analysis of the measured relative bed displacement for different aeration rates: glass ballotini, $f = 30$ Hz; $G = 1.25$.

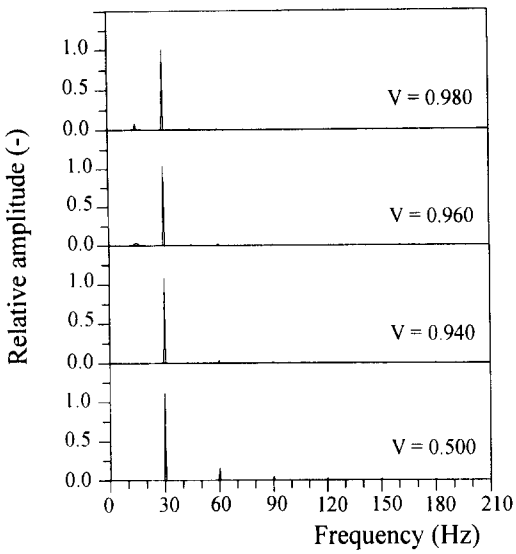

Fig. 16. Fourier analysis of the calculated relative bed displacement for different aeration rates: glass ballotini, $f = 30$ Hz; $G = 1.25$.

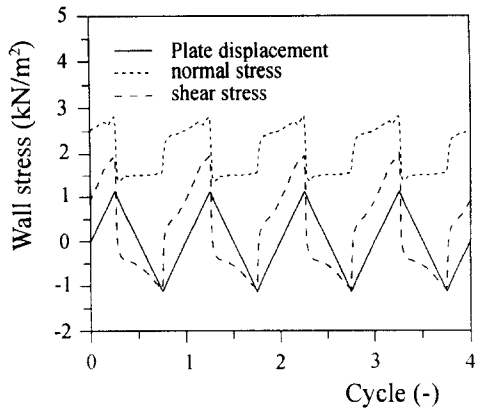

Fig. 17. Measured normal and shear stress of glass ballotini on the column wall for a triangular movement of the support plate: $f = 0.2$ Hz.

DISCUSSION OF SOME FEATURES OF THE SYSTEM NOT ACCOUNTED FOR IN THE MODEL

It is not impossible that the bed to some extent looses its coherence in the lower region during vibration. The pressure profiles in Fig. 5 show that under the conditions tested, only the bottom part of the bed experiences the fluctuating pressure profile. It is possible that the lower part of the bed will expand during rise, making it more permeable to the air, reducing the retracting pressure. In fact, reducing the retracting drag force by an empirical factor of 0.75 in the model, while maintaining the drag caused by aeration, it was possible to bring model predictions and experiment exactly into line.

Wall stress turned out to be extremely difficult to determine experimentally. When vibrating the support, vibrational movement was unavoidably passed on to the column wall, disturbing the measurements made with the load cells mounted on the inside of the wall (see Fig. 11). For this reason, an experiment was done at the extremely low frequency of 0.2 Hz using a triangular waveform rather than a sinusoidal one. The peak to peak movement of the plate was 4 mm.

The normal and shear stress acting on the wall are shown in Fig. 17, together with the movement of the support plate. The normal stress is taken as positive when compressive and the shear stress is positive when acting upwards. The bed height was 38.8 cm and the stresses were measured at 20.6 and 16.3 cm from the top of the bed. The normal stress clearly shows two stress levels: the active and passive states. When the moving support reverses its direction, the shear stress changes abruptly, but does not become constant during the period of constant support plate velocity.

Thus even at the simple experimental conditions above the variation of the wall/bed shear stress is complicated. It is, therefore, very difficult to account adequately for the influence of wall shear stress on the movement of a rapidly vibrating bed where only minor displacements are involved.

CONCLUSIONS

- A model has been developed for the motion of a vibrated bed of particles aerated through a porous support plate. This model has been solved numerically without making assumptions about the forms of the functions describing bed movement or pressure distribution.
- The effect of aeration through a porous support plate on the movement of the vibrated bed has been elucidated using the model. Increasing aeration causes the bed to come more loose from the support plate. At the higher aeration rates and vibration frequencies a peak in the Fourier transform of the bed movement at half the excitation frequency becomes evident. Porosity of the support plate has a similar effect in allowing the bed to come loose from the plate, since gas can enter into the developing gap between support plate and bed through the plate as well as from the bed. In the present investigation, though, the plate was so dense that this effect was not very significant.
- An experimental method, based on a porous disc moving with the bed, has been developed for direct measurement of the motion of a vibrated powder bed. This method has been shown to be viable, although problems with movement of the mechanical construction could not entirely be eliminated.
- Comparisons of measured and predicted bed motion in the frequency domain show good agreement for aerated beds. In particular the development of a Fourier peak in the bed movement at half the plate excitation frequency predicted by the model is also seen experimentally. The vibration intensity at which this starts is also reasonably well predicted.

— For non-aerated beds agreement between model and experiment was limited — perhaps due to the influence of wall friction — to the experimental trends being qualitatively consistent with theory.
— Lack of bed coherence, due to the non-uniform axial gradient in the pressure, may play a role. Reducing the retracting force of the bed to the plate by an empirical factor of 0.75 resulted in excellent agreement between model predictions and experiment.
— Initial experiments, in which the wall shear stress was measured under 'ideal' conditions, indicate that accounting for this in a model will not be straightforward.

NOTATION

A	cross-sectional area, m^2
d	particle diameter, m
f	vibration frequency, Hz
g	acceleration due to gravity, m/s^2
G	vibration number, dimensionless
h	time function, dimensionless
H	height or Fourier transform of h, m or dimensionless
$\tilde{H}$	discrete Fourier transform, dimensionless
I	time interval, s
k	permeability, m^2
m	integer variable, dimensionless
M	molecular weight of air, kg/mole
n	integer variable, dimensionless
N	number of data points, dimensionless
p	pressure, Pa
Δp	pressure drop over the bed, Pa
P	relative pressure, dimensionless
R	gas constant, J/mole K
s	width of the air gap, m
S	dimensionless width of the air gap, dimensionless
t	time, s
T	temperature, K
U	$= dS/d\tau$, dimensionless
v	superficial air velocity, m/s
V	dimensionless superficial air velocity, dimensionless
V_{pl}	volume beneath the support plate, m^3
x_o	amplitude of the support plate vibration, m
x	displacement of the bed, m
X	dimensionless displacement, dimensionless
z	distance from the top, m
Z	dimensionless distance, dimensionless

Greek letters

α	constant m^2/s
β	dimensionless constant, dimensionless
$\gamma_1,\gamma_2,\gamma_3$	dimensionless constants, dimensionless
ε	voidage, dimensionless
λ	dimensionless constant, dimensionless
μ	dynamic viscosity of air, Pa s
ν	dimensionless constant, dimensionless
ρ	density, kg/m^3
τ	dimensionless time, dimensionless
φ_v	volumetric air supply rate, m^3/s
ω	angular vibration frequency, 1/s
Ω	dimensionless angular vibration frequency, dimensionless

Subscripts

b	bed
c	collision
l	lift-off
mf	under conditions of minimum fluidization
o	at atmospheric conditions or of bottom plate
p	particles
pl	plate

REFERENCES

Akiyama, T. and Naito, T. (1987) Vibrated beds of powders: a new mathematical formulation. *Chem. Engng Sci.* **42**, 1305–1311.

Brigham, E. O. (1974) *The Fast Fourier Transform.* Prentice-Hall, Englewood Cliffs, NJ.

Erdész, K. and Halász, G. (1984) Hydrodynamic studies of fluidized beds. IX The mechanical analogous model of a vibrofluidized bed. *Hung. J. Ind. Chem.* **12**, 441–450.

Gray, W. A. and Rhodes, G. T. (1972) Energy transfer during vibratory compaction of powders. *Powder Technol.* **6**, 271–281.

Gutman, R. G. and Davidson, J. F. (1975) Darcy's law for oscillatory flow. *Chem. Engng Sci.* **30**, 89–95.

Gutman, R. G. (1976a) Vibrated beds of powders Part I: a theoretical model for the vibrated bed. *Trans. Instn Chem. Engrs* **54**, 174–183.

Gutman, R. G. (1976b) Vibrated beds of powders Part II: heat transfer and energy dissipation of a vibrated bed. *Trans. Instn Chem. Engrs* **54**, 251–257.

Kavetskii, G. D., Nikonov, L. V. and Krokhin, N. G. (1976) Aerodynamics of a vibroaeropseudofluidized bed. *Theor. Found. Chem. Engng* **10**, 830–833.

Kroll, W., 1954, Über das verhalten von schüttgut in lotrecht schwingenden fäsen. *Forschung* **20**, 2–15.

Marring, E., Hoffmann, A. C. and Janssen, L. P. B. M. (1994) The effect of vibration on the fluidization behaviour of some cohesive powders. *Powder Technol.* **79**, 1–10.

Pakowski, Z. and Strumillo, C. (1980) *Drying '80, Vol. 2, Proc. 2nd Int. Symp.*, Montreal Canada, 6–9 July 1980, ed. A. S. Mujumdar. Hemisphere, New York.

Thomas, B., Liu, Y. A., Chan, R. and Squires, A. M. (1987) A method for observing phase-dependent phenomena in cyclic systems. *Powder Technol.* **52**, 77–92.

Takahashi, H., Suzuki, A. and Tanaka, T. (1968/69) Behaviour of a particle bed in the field of vibration 1. Analysis of particle motion in a vibrating vessel. *Powder Technol.* **2**, t65–t71.

Wes, G. W. J. (1984) Ph.D. thesis, University of Groningen, The Netherlands.

Yamazaki, R., Kanagawa, Y. and Jimbo, G. (1974) Heat transfer in vibro-fluidized bed–effect of pulsated flow. *J. Chem. Engng Japan* **7**, 373–378.

Yoshida, T. and Kousaka, Y. (1967) Mechanism of vibratory packing of granular solids. *Kagaku Kogaku* **5**, 159–163.

APPENDIX A: EVALUATION OF THE MODEL EQUATIONS

A.1. *Nondimensionalization of the equations*

The model equations are rendered dimensionless by using the following variables and parameters:

$$Z_b \equiv \frac{z_b}{H_b} \quad Z_{\mathrm{pl}} \equiv \frac{z_{\mathrm{pl}}}{H_{\mathrm{pl}}} \quad P \equiv \frac{p}{p_o} \quad S \equiv \frac{s}{x_o} \quad \tau \equiv \frac{\alpha_b t}{H_b^2}$$

$$\gamma_1 \equiv \frac{\beta_b p_o H_b}{x_o \alpha_b} \quad \gamma_2 \equiv \frac{\beta_{\mathrm{pl}} A_{\mathrm{pl}} p_o H_b^2}{A_b H_{\mathrm{pl}} x_o \alpha_b} \quad \gamma_3 \equiv \gamma_2 \frac{A_b x_o}{V_{\mathrm{pl}}} \quad \lambda \equiv \frac{g H_b^4}{x_o \alpha_b^2}$$

$$\nu \equiv \frac{p_o H_b^3}{\rho_b x_o \alpha_b^2} \quad \Omega \equiv \frac{H_b^2 \omega}{\alpha_b} \quad \delta \equiv \frac{\alpha_{\mathrm{pl}} H_b^2}{\alpha_b H_{\mathrm{pl}}^2} \quad \psi \equiv \frac{\varphi_v H_b^2}{V_{\mathrm{pl}} \alpha_b} \qquad \text{(A1)}$$

where $\beta = k/\mu$ and the subscripts b and pl refer to the bed and the support plate, respectively. Three length scales, H_b, H_{pl} and x_o are used for the non-dimensionalization. This makes the resulting dimensionless equations slightly more complicated, but has as advantage that the terms retain their relative orders of magnitude. This is beneficial for the accuracy of the numerical computations.

The dimensionless equation of motion for the bed is:

$$\frac{\mathrm{d}^2 S}{\mathrm{d}\tau^2} = -\lambda + \nu(P_{Z_b=1} - 1) + \Omega^2 \sin(\Omega\tau). \qquad \text{(A2)}$$

The equations governing the pressure distribution in the bed and support plate become

$$\partial P/\partial\tau = \partial^2 P/\partial Z_b^2 \qquad \text{(A3)}$$

$$\partial P/\partial\tau = \delta(\partial^2 P/\partial Z_{\mathrm{pl}}^2) \qquad \text{(A4)}$$

with the dimensionless boundary conditions:

$$Z_b = 0: \quad P = 1 \qquad \text{(A5)}$$

$$Z_b = 1: \quad (\mathrm{d}S/\mathrm{d}\tau) = -\gamma_1(\partial P/\partial Z_b) + \gamma_2(\partial P/\partial Z_{\mathrm{pl}}) \qquad \text{(A6)}$$

$$Z_{\mathrm{pl}} = 1: \quad (\mathrm{d}S/\mathrm{d}\tau) = \psi - \gamma_3(\partial P/\partial Z_{\mathrm{pl}}). \qquad \text{(A7)}$$

For the case where the bed is in contact with the support plate, the boundary condition for the bottom of the bed and the top of the support plate is in dimensionless form:

$$Z_b = 1 \text{ and } Z_{\mathrm{pl}} = 1: \quad \gamma_1 \frac{\partial P}{\partial Z_b} = \gamma_2 \frac{\partial P}{\partial Z_{\mathrm{pl}}} \qquad \text{(A8)}$$

while the boundary conditions at the top of the bed and bottom of the support plate remain the same.

A.2. *The numerical calculation scheme*

The starting condition is at $t = \tau = 0$ with atmospheric pressure everywhere in the bed: $p = p_o$ ($P = 1$). The bed is in contact with the support plate.

Under these initial conditions an air gap will develop only if $G > 1$. When this occurs the bed looses contact at a certain time t_l, which is easily calculated. From then on the set of equations applying to the bed in flight has to be solved. To this end the diffusion eq. (A3) and its counterpart for the support plate (A4) are, together with the boundary conditions, written in finite difference form using a central differencing scheme.

Instead of using the second-order equation (A2) directly, a new variable is introduced: $U \equiv \mathrm{d}S/\mathrm{d}t$. The set of equations resulting from the discretization of the diffusion equations are therefore supplemented with the discretized form of the two following equations, which together represent the equation of motion of the powder bed.

$$U = \mathrm{d}S/\mathrm{d}\tau \qquad \text{(A9)}$$

$$\mathrm{d}U/\mathrm{d}\tau = -\lambda + \nu(P_{Z_b=1} - 1) + \Omega^2 \sin(\Omega\tau). \qquad \text{(A10)}$$

These equations are also discretized using a central differencing scheme. In this way the diffusion equations with the boundary conditions and the equation of motion are brought together into a single set of linear equations. This set of equations form a sparse matrix which is solved using Gaussian elimination with partial pivoting.

Proceeding now with the calculation in time using an appropriate time step, the set of equations is solved continuously until the air gap closes. The time the bed makes contact with the plate, t_c, is calculated iteratively to ensure accurate starting conditions for the calculation of the bed movement after t_c.

At the contact time t_c an inelastic collision is assumed which means that the velocity and displacement of the bed are put equal to that of the support plate at the time of impact.

Two scenarios can then occur, depending on the acceleration of the plate at t_c: (a) the bed lifts off again immediately or (b) remains in contact with the plate for some time. In case an air gap is formed immediately, the set of equations remains the same and the initial conditions are the calculated pressure distribution at t_c, $S = 0$ and $U = \mathrm{d}S/\mathrm{d}\tau = 0$.

If the bed remains in contact with the support plate, however, the set of equations being solved changes to the one applying to that situation, which is then solved from t_c on, with the pressure distribution at t_c as initial condition.

For each time step the acceleration of bed and plate are compared and at a new iteratively calculated time t_l the bed lifts off from the support plate again. In this way the calculations are continued until t has reached the value of approximately four seconds. Only the last two seconds are used for evaluation in order to avoid including start-up behaviour.

Since we are following the time-dependent behaviour, the solution was checked for both independence of the magnitude of the time-step and of the fineness of the spatial grids in the bed and the support plate. Also known solutions for the case of an impermeable support plate were correctly reproduced.

APPENDIX B: PROCESSING OF THE DATA FROM THE LVDT

The data from the LVDT was converted to the frequency domain using a fast Fourier Transform (FFT) algorithm. This has as advantage that noise from the power supply and other sources can be eliminated. Moreover, the random error generated in digitalizing the LVDT signal, which is of no particular frequency, does not obscure the relevant data. Viewing the data in the frequency domain also allows the detection of lower or higher harmonics, difficult to identify in the time domain.

Since the plate movement is sinusoidal, it is described by eq. (1), and we use the dimensionless vibration intensity, G, defined in eq. (2).

The Fourier transform of the waveform $h(t)$ is defined as:

$$H(f) \equiv \int_{-\infty}^{\infty} h(t)\, \mathrm{e}^{-j2\pi ft}\, \mathrm{d}t. \qquad \text{(B1)}$$

For the integral to be defined, the function h has to satisfy certain criteria. In practice, it has to be continuous. In our

case, where only sampled data are available, a 'discrete' Fourier transform can be calculated from N data points sampled with an interval I:

$$\tilde{H}\left(\frac{n}{NI}\right) \equiv \sum_{m=0}^{N-1} h(mI)\,e^{-j2\pi nm/N}, \quad n = 0,1, \ldots, N-1 \quad \text{(B2)}$$

where $h(mI)$ represents the sampled data and $\tilde{H}(n/NI)$ is the discrete Fourier transform at the frequency (n/NI) (Brigham, 1974).

The Fourier transform of sampled values of a periodic time function will approximate the continuous Fourier transform optimally if: (a) the waveform has a band-limited frequency spectrum and the sampling rate is at least twice the highest frequency component and (b) the total sampling period covers an integer multiple period of $h(t)$. The discrete Fourier transforms were calculated using a fast Fourier algorithm.